THz imaging and sensing for security applications—explosives, weapons and drugs

2005 Semicond. Sci. Technol. 20 S266

(http://iopscience.iop.org/0268-1242/20/7/018)

INSTITUTE OF PHYSICS PUBLISHING SEMICONDUCTOR SCIENCE AND TECHNOLOGY
Semicond. Sci. Technol. **20** (2005) S266–S280 doi:10.1088/0268-1242/20/7/018

THz imaging and sensing for security applications—explosives, weapons and drugs

John F Federici[1], Brian Schulkin[1], Feng Huang[1], Dale Gary[1], Robert Barat[2], Filipe Oliveira[2] and David Zimdars[3]

[1] Department of Physics, New Jersey Institute of Technology, Newark, NJ, USA
[2] Otto York Department of Chemical Engineering, New Jersey Institute of Technology, Newark, NJ, USA
[3] Picometrix Inc., Ann Arbor, MI, USA

Received 29 March 2005
Published 8 June 2005
Online at stacks.iop.org/SST/20/S266

Abstract
Over the past 5 years, there has been a significant interest in employing terahertz (THz) technology, spectroscopy and imaging for security applications. There are three prime motivations for this interest: (a) THz radiation can detect concealed weapons since many non-metallic, non-polar materials are transparent to THz radiation; (b) target compounds such as explosives and illicit drugs have characteristic THz spectra that can be used to identify these compounds and (c) THz radiation poses no health risk for scanning of people. In this paper, stand-off interferometric imaging and sensing for the detection of explosives, weapons and drugs is emphasized. Future prospects of THz technology are discussed.

(Some figures in this article are in colour only in the electronic version)

1. Introduction

1.1. The lure of terahertz

Over the past several years, there has been an increased interest in the potential of terahertz (THz) detection for imaging of concealed weapons, explosives and chemical and biological agents. There are three major factors contributing to this interest.

(a) Terahertz radiation is readily transmitted through most non-metallic and non-polar mediums, thus enabling THz systems to 'see through' concealing barriers such as packaging, corrugated cardboard, clothing, shoes, bookbags, etc in order to probe the potentially dangerous materials contained within.
(b) Many materials of interest for security applications including explosives and chemical and biological agents have characteristic THz spectra that can be used to fingerprint and thereby identify these concealed materials.
(c) Terahertz radiation poses either no or minimal health risk [1–5] to either a suspect being scanned by a THz system or the system's operator.

As plastic explosives, fertilizer bombs and chemical and biological agents increasingly become weapons of war and terrorism, and the trafficking of illegal drugs increasingly develops as a systemic threat, effective means for rapid detection and identification of these threats are required. One proposed solution for locating, detecting and characterizing concealed threats is to use THz electromagnetic waves to spectroscopically detect and identify concealed materials through their characteristic transmission or reflectivity spectra in the range of 0.5–10 THz. For example, many explosives (for example, C-4, HMX, RDX and TNT) and illegal drugs (for example, methamphetamine) have characteristic transmission/reflection spectra in the THz range that could be distinguishable from other materials such as clothing, coins and human skin. In essence, these materials should appear as different 'colours' to the THz detector as compared to non-hazardous items. Using THz spectroscopy it should be possible to detect explosives or drugs even if they are concealed, since the THz radiation is readily transmitted through plastics, clothing, luggage, paper products and other non-conductive (non-metallic) materials. By comparing measured reflectivity THz spectra with known calibration

spectra, one may identify the presence of these agents and distinguish them from benign objects.

1.2. THz versus millimetre wave imaging

Millimetre wave (MMW) imaging [6] is a fairly well-developed technology. Typically, MMW systems operate at a discrete operation frequency of roughly 30 GHz (300 GHz corresponds to 1 mm wavelength). While MMW systems penetrate better through some barrier materials compared to THz systems, there are two important considerations that favour THz scanning for security applications: (a) spatial resolution and (b) spectroscopic signatures. Terahertz detection inherently has a roughly ten times better spatial resolution compared to MMW systems simply because the electromagnetic wavelength of THz radiation is roughly ten times shorter than MMW radiation. Consequently, images of suspicious objects such as concealed metallic or plastic knives are much sharper and more readily identified when imaged with THz scanners [7]. A second important consideration is specificity. Through known characteristic THz spectra of explosives, biological and chemical agents and illegal drugs, a THz image can be spectroscopically analysed to identify concealed contents and potential threats. This capability is particularly important for explosives, for example, that have low vapour pressures and therefore would pose a challenge to trace vapour detection techniques. Comparable spectroscopic 'fingerprint' spectra of these threats are not present in the MMW range.

1.3. Scope of article

This paper will focus on the interferometeric imaging approach to employing terahertz technology for security applications such as the detection of concealed explosives, weapons and drugs. Section 2 discusses THz spectroscopy as it applies to these threats as well as to remote detection through the atmosphere and the transmission of THz through barrier materials. Section 3 discusses several configurations of THz systems: transmissive versus reflective detection, pulsed THz detection systems versus continuous wave (CW) THz detection systems and close proximity versus stand-off detection. Section 4 discusses the use and advantages of a synthetic aperture approach to THz imaging. Section 5 discusses two THz spectral analysis techniques. In section 6, the challenges and future prospects for THz in the security field are discussed.

2. THz spectra

The ability of THz light to interact differently with benign and threat materials as a function of THz frequency yields a highly flexible foundation for THz imaging security screening based on spectroscopy. In general, non-polar, non-metallic solids such as plastics and ceramics are at least partially transparent and reflective in the 0.2–5 THz range. Non-polar liquids are transparent as well, whereas polar liquids, such as water, are highly absorptive. This is because absorption in the THz range of the electromagnetic spectrum is generally due to the rotational motions of dipoles within a material. Crystals formed from polar liquids are substantially more transparent because the dipolar rotations have been frozen out; however, these crystals may exhibit phonon resonances in the THz range. Terahertz time-domain spectroscopy (TDS), Fourier transform infrared (FTIR) experiments and computer simulation of the far-infrared spectra of organic molecules show vibrational features associated with intermolecular hydrogen bond relative motions [8–10]. Gases can have distinctive spectroscopic fingerprints in the THz range [11].

The THz imaging technique is based on the use of THz electromagnetic waves to spectroscopically detect and identify concealed explosives, chemical and biological agents and illegal drugs through their characteristic transmission or reflectivity spectra in the THz range. Experimental data have appeared in the literature that suggest that many materials that are relevant to security applications have characteristic THz reflection or transmission spectra (see references listed in table 1). Typical clothing items and paper and plastic packaging should appear transparent in the THz regime. Metals completely block or reflect THz waves. Ceramic guns and knives would partially reflect the THz light. Skin, because of its high water content, would absorb nearly all T-rays. The energy would be harmlessly dissipated as heat in the first 100 μm of skin tissue. A THz reflection image of a person would show the outline of clothing and the reflection of objects beneath (such as weapons or key chains), but the person's skin would appear substantially dark.

This section summarizes the THz spectra of three major classes of materials: the targeted explosives and illicit drugs, barrier materials that could conceal the targeted materials and the atmosphere. Atmospheric transmission of THz radiation is particularly important for stand-off sensing.

2.1. Sample preparation

Before discussing the THz spectra, some detailed notes should be made regarding sample preparation. There are several methods for preparing samples for spectroscopic testing. Ideally, for security applications, the THz spectra should be independent of sample preparation. However, the sample preparation method can have minor or substantial effects on the THz spectra. The reason is that the THz spectra can be sensitive to the preparation method, structural changes of the material or to impurities/fillers that are introduced during sample preparation. As an example, there are discrepancies in the THz spectra of RDX as reported in [12–14]. In addition, the experimental method itself can introduce spectral artefacts that can mask the true THz spectral fingerprint. These include multiple reflections within the sample, multiple reflections between the sample and its holder, multiple reflections from the system, etc [15].

To uniquely identify the intrinsic feature of the material, one method of sample preparation is to pelletize the explosive powders/crystals [16]. It is standard practice in far-infrared (THz) spectroscopy to press samples into pellet form in order to measure the THz transmission spectra. When the sample is a powder with a grain size comparable to the THz wavelength (about 300 μm), the powder strongly scatters the THz radiation. Another method of sample preparation is to mix the material (e.g. RDX) with an inert matrix or filler

Table 1. Collection of absorbance peak positions of some explosives and drugs. Conversion to units of wavenumbers requires multiplication by 33 $cm^{-1} = 1$ THz.

Material	Feature band centre position frequency (THz)	Reference
Explosive		
Semtex-H	0.72, 1.29, 1.73, 1.88, 2.15, 2.45, 2.57	[12]
PE4	0.72, 1.29, 1.73, 1.94, 2.21, 2.48, 2.69	[12]
RDX/ C4	0.72, 1.26, 1.73	[12, 14, 27]
PETN[a]	1.73, 2.51	[12]
PETN[b]	2.01	[16]
HMX[a]	1.58, 1.91, 2.21, 2.57	[12]
HMX[b]	1.84	[16]
TNT[a]	1.44, 1.91	[12]
TNT[b]	1.7	[16]
TNT	5.6, 8.2, 9.1, 9.9	[20, 27]
NH_4NO_3	4, 7	[16, 22]
Drugs		
Methamphetamine	1.2, 1.7–1.8	[23]
MDMA	1.4, 1.8	[23]
Lactose α-monohydrate	0.54, 1.20, 1.38, 1.82, 2.54, 2.87, 3.29	[12]
Icing sugar	1.44, 1.61, 1.82, 2.24, 2.57, 2.84, 3.44	[12]
Co-codamol	1.85, 2.09, 2.93	[12]
Aspirin, soluble	1.38, 3.26	[12]
Aspirin, caplets	1.4, 2.24	[12, 23]
Acetaminophen	6.5	[19]
Terfenadine	3.2	[19]
Naproxen sodium	5.2, 6.5	[19]

[a] Samples are prepared as pellets using spectrographic-grade polyethylene.
[b] Samples are ordered as compressed pellets from Accurate Energetics LLC. All materials are in sensitized form (water-free).

material to create a pellet. The filler is typically a material that is transparent in the THz, such as polyethylene. This allows dilute concentrations of a highly absorbing agent to be measured.

The presence of a matrix material and/or a pressed pellet, however, can influence the measured THz spectra. For example, the use of a matrix material with an index of refraction that closely matches that of the powder can minimize the scattering by reducing the effect of the dielectric mismatch in the THz range. In general, one would need to analyse the spectroscopic data that treat the composite sample as one dielectric material (powder) imbedded in another dielectric host material (Garnett theory) [17]. The proximity of grains of powder to each other can lead to interaction between neighbouring grains that modifies effective dielectric of composite material and consequently the THz spectra [18]. It has been suggested [14] that several of the THz peaks in RDX are due to crystalline nature of the powder and long-range oscillations of the crystal structure. In order to conduct a thorough experiment with pellets, one should try different fillers, packing fractions, etc to ensure that the spectral features of interest are not artefacts resulting from a particular form of sample preparation.

While it is good science to pelletize samples to try to understand the scientific origin of various THz peaks, terrorists or smugglers are not going to prepare their samples so that they are readily detectable! A realistic fieldable THz detection system should be able to measure/detect the threat in a realistic form (e.g. ammonium nitrate right out of the bag) or in a realistic filler (e.g. RDX in a plastic matrix to make C4). In spite of varying preparation methods, many spectral features of explosives, for example, are reproducible and not sensitive to sample preparation. While there are some slight variations in the THz spectra of C4 and RDX that can be attributed to the matrix or sample preparation methods, there are clearly peaks/features in the THz spectra that are independent of whether one is measuring an RDX grains, powder or RDX mixed in a matrix (e.g. C4).

2.2. Explosives

Table 1 contains an abbreviated summary of materials with their reported absorbance peak positions. A dominant feature of the THz spectra is the sharp absorption peaks caused by phonon modes directly related to the crystalline structure [16]. This result originates from the molecular vibrational modes and intramolecular vibrations associated, for example, with RDX [14]. Consequently, vibrational modes are unique and distinctive feature of the crystalline explosive materials. The presence of broad features might be caused by scattering from a structure with dimensions comparable to the THz wavelength. This usually occurs in materials that contain fibres or grains [19].

Note that there are several absorption features from 0 to 5 THz that can be used to uniquely identify the explosive/drug. For the most part, there is good agreement between the spectral features as measured by different groups. In particular, figure 1 shows a comparison of the THz spectra of RDX and C4 from [14, 13]. Note that the absorption features at 0.8, 1.5, 2.0, 2.2 and 3 THz are exhibited in both the datasets. It should be noted that the main absorption features of RDX are still present when RDX is mixed with a matrix material to make

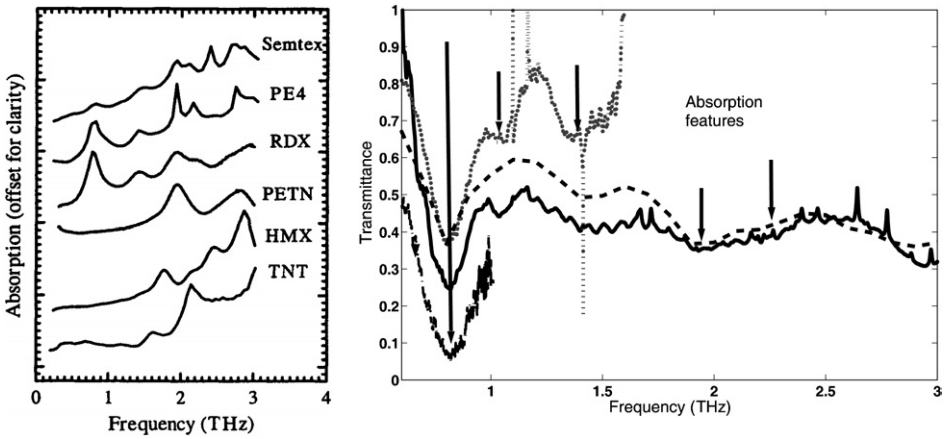

(*a*) (*b*)

Figure 1. (*a*) THz absorption spectra from [13]. (*b*) Comparison study of transmission spectra of RDX using THz-TDS and FTIR (Fourier transform infrared) spectroscopy with data from [13, 14]. The dashed line is RDX from [13]. The other curves are from [14] where the bottom curve is RDX measured by THz-TDS, the solid curve is RDX measured by FTIR, and the top curve is C4 measured by THz-TDS). The sharp features in C4 (THz-TDS) are remnants of water. Note that the absorption features at 0.8, 1.5, 2.0, 2.2 and 3 THz are exhibited in both the datasets. The spectral feature at 1.1 THz is not present in both datasets.

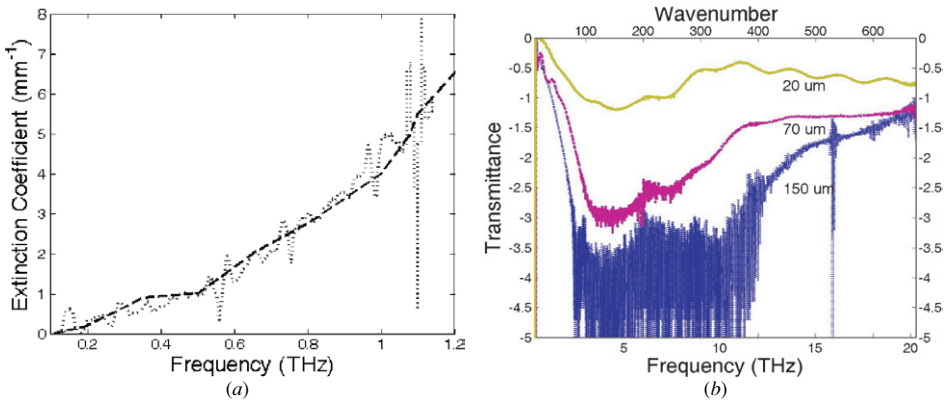

(*a*) (*b*)

Figure 2. (*a*) THz spectra of ammonium nitrate (1 mm thick sample). The dotted line corresponds to measured data of [22]. The dashed line is from [16]. (*b*) Extended transmission spectra [22] out to 21 THz with nominal sample thickness listed.

C4. The spectral feature at 1.1 THz from [14] is not present in the data from [13].

As an example of the THz spectral assignment of peaks in crystalline explosives, the THz spectra of RDX [14] and TNT [20] have been compared with a SPARTAN *ab initio* molecular simulations [21] study using density function theory. The TNT molecular vibrational modes >5 THz agree well with the measured THz absorption. Major spectral features should not exist below 1 THz for known molecular conformations of RDX. *Ab initio* calculation of the vibration modes of one single RDX molecule compared well with the experimental FTIR data beyond 600 cm^{-1} [21]. The observed 0.8 THz feature of RDX (see figure 1) is interesting since it does not appear to correspond to an inherent molecular vibrational mode. It is therefore reasonable to attribute this significant absorption feature at ∼0.8 THz to interactions between the RDX molecules. Possible explanations include molecular conformations (e.g. partial rotations of the nitro (–NO_2) groups), the acoustical branch of such interaction, a weak hydrogen bond between two RDX molecules or a partial rotation of the RDX molecule.

The first nine explosives listed in table 1 show distinct THz fingerprints in the 0.1–3 THz range. Since these explosives typically have low vapour pressure [16], THz spectroscopy offers a potentially useful detection method alternative to those techniques that require a relatively high vapour pressure.

This leaves open issue of detecting amorphous explosives (versus high-grade crystalline explosives such as RDX) using THz. One of the few reported explosive materials that do not contain sharp features, but instead a monotonically increasing attenuation in the 0–3 THZ range is ammonium nitrate (AN) [16, 22]. This is unfortunate because AN mixed with fuel oil (FO) is a prolific 'dirty' explosive that is commonly used as an improvised explosive device (IED) for truck/car bombs.

Figure 2 shows our experimentally measured THz spectra of AN compared with the data of [16]. The data show an increasing THz absorption (extinction coefficient) as the THz frequency increases up to ∼3 THz. Two subtle oscillations appear in the spectra in the 3–7 THz range. (The ∼70 cm^{-1} wide oscillations in the transmission from 10 to 20 THz for the 20 μm sample are due to multiple reflections in the sample.) Unlike the THz spectra of RDX, which show several spectral features that can be used to uniquely identify RDX in the 0.2–3 THz range, ammonium nitrate does not exhibit any such distinguishing spectral features except for the broad spectral absorption peaking at ∼3 THz.

The THz detection of ammonium nitrate as well as other 'featureless' explosives requires special consideration. Clearly, one option is to design a THz system that operates in the 3–7 THz range (assuming the availability of sources and detectors) where a 'fingerprint' spectra might be present. The second option is to detect the FO component of the ANFO explosive (if present). The third option would be to identify the material based on the slope of the increase in THz absorption in the 0.2–3 THz range. The fourth alternative is to make two measurements: one at 0.2 THz and another at roughly 2.5 THz. At the lowest frequency, ammonium nitrate is essentially transparent while it is essentially opaque at the higher frequency. While this last alternative would not specifically identify the presence of AN, it would provide a quick test (simple yes/no answer) to determine if the THz transmission/reflection is consistent with the presence of AN.

2.3. Illicit drugs

While the literature on THz spectroscopy of explosives is quite extensive, the corresponding studies of THz spectroscopy for sensing applications of illegal drugs [23] have been much more limited. (There have been more THz spectra reported in the literature for legal drugs [13, 23, 24].) As with the detection of explosives, THz spectroscopy shows great promise due to its ability to 'see' through most packaging material to probe for the presence of illicit drugs that exhibit a characteristic THz spectral fingerprint. Competing detection technologies such as x-rays and millimetre wave imaging lack a spectral fingerprint in their respective electromagnetic frequency ranges to distinguish illicit drugs from common/legal drugs [23]. Infrared imaging has the capability to distinguish different drugs based on fingerprint spectra in the infrared region, but most packaging materials (e.g. envelopes, cardboard, etc) are opaque to probing in the infrared.

Using a discretely tunable THz source, Kawase *et al* [23] imaged methamphetamine, MDMA (DL-3,4-methylenedioxymetamphetamine) and common aspirin as a reference. The major THz absorption peaks in the 1.3–2 THz range in these drugs are as shown in table 1. About 20 mg of each drug was individually placed in polyethylene bags and hidden in an envelope. THz images were recorded at seven different THz frequencies and analysed using component spatial pattern analysis [25]. The analysis showed an error of roughly 10%. Kawase *et al* have also demonstrated that they can identify extract the spatial patterns of the different drugs even when they are mixed together or stacked on top of each other. (This is an important consideration for security applications where people would intentionally attempt to confuse a THz sensing system.) Kawase also reports characteristic THz spectra for D-amphetamine, L-ephedrine and L-methylephedrine, and over-the-counter drugs L-methamphetamine, acetaminophen (Tylenol) and caffeine [23].

2.4. Barrier materials

Under realistic circumstances, a target threat material will be concealed in a package, under clothing, etc. Such 'barrier' materials that conceal the threat material have their own characteristic THz transmission spectra that must be taken into account. For example, a barrier material might absorb THz radiation and therefore limit the maximum thickness of material that the THz can 'see through'. It is also possible that the barrier material could exhibit similar THz absorption peaks ('colours') which could mask the spectral characteristics of the explosives or illicit drugs. However, most barrier materials such as cloth, paper and plastic show a THz absorption spectra that is gradually increasing with frequency, particularly below 3 THz [13, 19, 24, 26].

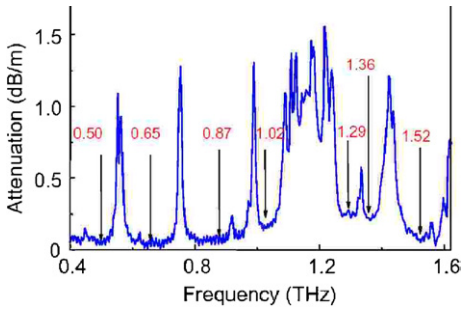

Figure 3. Atmospheric transmission bands in the terahertz range of frequencies (after [8]).

The detection of land mines using THz spectroscopic imaging [20, 27] has some unique considerations in terms of barrier materials. Currently, there are an estimated 100 million landmines buried worldwide. Anti-personnel mines are small devices and contain minimal amounts of metal. Ground penetrating radar systems, due to limited spatial resolution, cannot distinguish these small mines from rocks. THz technology with roughly a factor of 10 better spatial resolutions (∼1 mm) should provide better discrimination.

Detection of landmines requires THz to propagate through sand and soil. It is anticipated that imaging through such grainy and moist material will significantly affect the detectability of non-metallic objects hidden beneath it. Sand is measured to have a loss of 8.2 dB cm^{-1}%, where % denotes the water weight percentage. The non-metallic landmine detection proof of concept was done by imaging a Neoprene grommet (OD = 25.4 mm, ID = 12.7 mm) under 1.2 cm of dry sand [20]. An image is formed by scanning every 300 μm for 100 × 100 pixels. The grommet can clearly be seen in the image.

2.5. Atmosphere

Both close proximity (<3 m) and stand-off detection (>3 m) of concealed threat materials require consideration of THz transmission through barrier materials. A stand-off THz detection system must be capable of propagating short (3–100 m) distances through the atmosphere. Terahertz propagation through the humid atmosphere has been discussed by several groups [8, 11, 28]. Atmospheric absorption, which is dominated by water and oxygen as one moves from the millimetre to the THz range [11], absorbs THz radiation at specific frequencies. However, there are numerous transmission bands throughout the THz frequency range as shown in figure 3 [8]. While the THz attenuation in the transmission bands is frequency dependent, a typical number is 50 dB km^{-1} at 0.8 THz. A stand-off sensing system should be tuned to these transmission bands to minimize the absorptive losses of THz radiation by the atmosphere. While

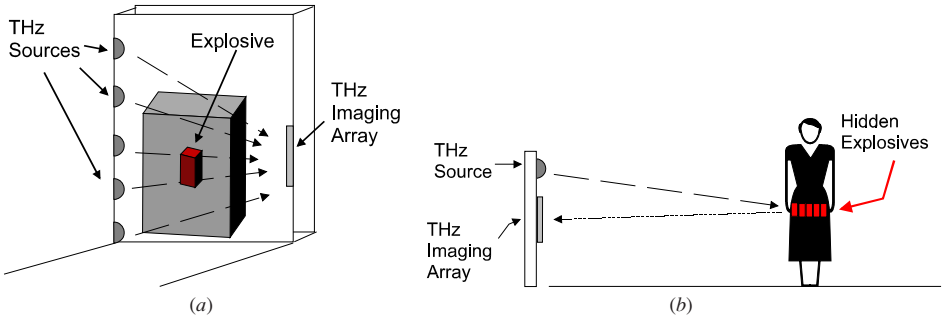

Figure 4. Illustration of a potential implementation of a THz imaging array in transmission mode (*a*) and reflection mode (*b*).

atmosphere attenuation is predominately due to absorption of the THz radiation by water vapour, other attenuation effects such as dust, smoke, fog and rain could affect the THz transmission. It is thought that rain would increase the effective attenuation due to increased water absorption, while typical micron-scale particles, such as dust, pollens and smoke, would not greatly scatter the THz radiation [28] since the THz wavelength is much longer than typical micron-scale particles. However, there are little or no experimental data on atmospheric scattering of THz radiation [28].

3. THz detection systems

In this section we discuss several important issues that must be considered in developing a THz detection system for security applications.

3.1. Transmission versus reflective geometry

Figure 4 shows a schematic of two possible implementations: a transmission mode and a reflection mode. In both cases, THz sources illuminate a person or pallet under study. In the transmission mode, the THz radiation propagates through the material to be inspected to the receiving detector. Since many explosive materials strongly absorb THz radiation, a transmission mode is effective for fairly small quantities of explosives (e.g. about 0.1 mm thick slab of RDX or about 20 mg of illicit drugs). Much thicker samples become virtually opaque to the THz. In this case, a reflection mode is preferred. In this scenario, a bright THz source illuminates the person under study, for example. The THz radiation propagates through the clothing, reflects from the hidden explosive, propagates back through the clothing and is finally detected.

While many transmission spectra of explosives have been measured, there have been few reported measurements on reflection spectra [29–31]. Zhang *et al* [30] showed for the case of 2,4-DNT that characteristic spectral peaks appear in both the transmission and reflection spectra at the same wavelength. A simple Kramers–Kronig argument suggests that this is reasonable: rapid changes in the THz transmission as a function of frequency can be attributed to rapid changes in the imaginary index of refraction (absorption coefficient). By Kramers–Kronig transformations, rapid changes in the imaginary index of refraction are exhibited in the real index of refraction. Since the reflectance of a material is determined by the real and imaginary indices of refraction, rapid changes in the imaginary index of refraction should be exhibited in both the transmission and reflection measurements. However, the reflectivity of an object depends not only on the indices of refraction, but also on the surface roughness, polarization of the incident THz radiation and other geometric factors. Considering that a reflective geometry is essential for detecting explosives and other threats on a person, experiments confirming that the characteristic spectra in transmission show similar features in reflection have been undertaken [31].

3.2. Close range versus stand-off detection

The simplest method of THz imaging is to use a single transmitter and detector—i.e. line-of-sight detection. An image is obtained on a point-by-point basis by scanning the transmitter/detector pair over the sample under test and recording the THz phase and amplitude at each point. Using this method, THz images of macroscopic objects have been obtained [32] and extended to THz tomography [33] and synthetic phased-array techniques [34, 35].

Close range (<3 m) imaging offers solutions to a wide variety of applications. Over short distances, atmospheric attenuation and scattering are minimal. Screening of mail, packages and baggage is a close range application, whereas detection of explosives, weapons and illicit drugs on people approaching a check-point or portal is a stand-off application. Close range imaging has been greatly studied. The three main techniques, each having different meritorious properties [35], areas follows:

- *Raster scanning.* A tightly focused THz beam is scanned across the surface of a thin sample. The reflected [36] or transmitted [33] THz is measured and an image is produced on a pixel-by-pixel basis.
- *Impulse scanning* [37]. Time-delayed THz signals are used to stack an image. This technique provides fine transverse resolution.
- *Electro-optic imaging* [38, 39]. THz images are shifted into visible light, allowing conventional CCD cameras to acquire images at a very rapid rate. The trade-off for the speed is low dynamic range; small or weakly reflecting signals cannot be imaged.

The main disadvantage of close range imaging is the frame rate. Other than electro-optic imaging, which provides a poor dynamic range, these systems may not be implemented as turnkey, video-rate scanning systems. A high speed THz imaging device that can scan and positively identify harmful materials at video frame rates is in high demand for security

applications. Stand-off (>3 m) THz imaging allows for long-range screening and detection and potentially offers a solution for scanning persons in open areas such as airports, stations, etc.

The two main imaging techniques that have potential for stand-off imaging are focal plane array and interferometric imaging. A focal plane array approach is similar to a standard CCD optical camera, where each detector denotes a pixel in the image. Due to the high expense of THz detectors and limited detector packing density, it is not practical to fabricate an array of 1920 000 (1600 × 1200) pixels. Instead, a line camera, equivalent to a flatbed scanner, could be scanned over a region comprising the mega-pixel imaging element. The scanning action decreases the frame rate dramatically, rendering a real challenge for real-time detection. Interferometric imaging, unlike focal plane arrays, uses intensity and phase information between pairs of detectors. The distance between each pair is referred to as a baseline, and the image quality is strictly dependent on utilizing a wide range of unique baselines. For N detectors, there are $N(N-1)/2$ detector pairs corresponding to $N(N-1)/2$ pixels in a reconstructed image. Consequently, fewer detectors and faster frame rates are needed for the interferometric approach as compared to the focal plane array approach.

3.3. Pulsed versus CW sensing

THz imaging approaches have typically used either short-pulsed laser or continuous wave (CW) difference frequency THz generation and detection. CW generation of THz radiation by photomixing (beating) of two infrared laser sources commenced in the 1990s through the seminal work of Brown, McIntosh and Verghese [40]. The technology for growth, design and characterization of the low-temperature (LT) grown GaAs photomixers has improved dramatically [40, 41], enabling the use of CW THz systems for sensing, spectroscopy [28, 42] and imaging applications [43–47]. The key materials component of LT-GaAs and higher power ErAs:GaAs photomixers is the presence of nanoparticulates that reduce the charge carrier lifetime in the material to the sub-picosecond level thereby enabling optical mixing to the THz range. While there have been improvements in photomixer performance with ErAs:GaAs materials [48], the photomixer approach has been limited by the achievable output power and device reliability [49]. To circumvent the carrier lifetime limits of the GaAs system, several groups utilized p–i–n photodiode structures [49]. Terahertz photomixing by resonant excitation of plasma oscillations in quantum well structures has also been considered [50]. While the GaAs system uses infrared lasers at ∼800 nm wavelengths, the InAlAs/InGaAs system can utilize inexpensive telecommunication lasers operating near 1.5 μm [51]. In addition to semiconductor-based systems, CW THz generation and detection have been demonstrated using nonlinear optical crystals [52].

An example of quasi CW THz detection for detection of illicit drugs [23] uses a THz wave parametric oscillator (TPO) consisting of Q-switched Nd-YAG laser and parametric oscillator [25, 53]. In this technique, MGO:$LiNb_3$ is employed as a nonlinear material to generate CW THz. Silicon prisms couple the THz radiation from the nonlinear crystal where it is detected using a pyroelectric detector. THz images are collected at discrete THz frequencies and then spectroscopically analysed using a component spatial pattern analysis method to determine sample composition.

The short-pulsed laser method usually involves the generation and detection of THz pulses using either photoconductive antenna structures or optical rectification in a nonlinear crystal. In one version of the short-pulsed laser technique [39], the entire waveform of a single THz pulse is recorded by encoding the temporal profile of the THz pulse on a chirped ultra-fast laser pulse. Each infrared wavelength length of the infrared laser pulse corresponds to a different time window of the THz pulse. The temporal profile of the THz pulse is measured by analysing the spectral components of the infrared pulse. In the CW generation method, two narrowband infrared laser sources are miss-tuned by roughly 1 THz. Continuous wave THz radiation is generated by mixing of two laser sources in a nonlinear crystal. One limitation in utilizing these techniques is that coherent CW or short-pulsed laser sources are required. Moreover, the laser sources that generate and detect the THz radiation must retain a coherent phase relationship with each other. Using these methods, the imaging of an incoherent THz source is not possible.

Pulsed sources seem to be more favourable (in particular for close proximity applications) because they can be used for acquiring depth information. For example, a pulsed THz imaging method was used [7, 12, 13, 54] to demonstrate a proof of principle for security screening. Hidden objects (for example, scalpel, alumina ceramic, acrylic plastic and SX2 sheet explosive) were imaged through barrier materials (for example, inside a parcel post box or under layers of clothing or shoes). The advantages of pulsed THz time-domain spectroscopy are that broad spectral information (0.1–3 THz) can be acquired from a single picosecond THz pulse as well as the depth information from the difference in arrival times of the short pulses. CW imaging systems have the advantage of higher THz power at a distinct THz frequency. A further advantage of CW THz spectroscopy over pulse THz time-domain spectroscopy is that narrow spectral features are easier to measure using CW techniques due to the inherently spectrally narrow CW THz radiation and due to the lack of a long scanning delay line that would be required for high spectral resolution using a time-domain system.

3.4. Stand-off sensing modalities

For stand-off detection, a dominating issue in choosing a pulsed or continuous wave source is the need to propagate through the atmosphere. As discussed in section 2, only certain bands of THz frequencies are appropriate transmission windows for remote detection applications. For THz time-domain pulses that are generated by short-pulse laser systems (e.g., mode-locked Ti:Sapphire laser), the THz spectrum of the pulse spreads over several transmission bands. However, the THz power which is *outside* the transmission bands is highly absorbed. Consequently, the amount of usable THz power in the pulse is drastically reduced. In addition, the time duration of the picosecond THz pulses is considerably lengthened due to water absorption rendering pulsed time-of-flight THz detection impossible. For propagation of THz

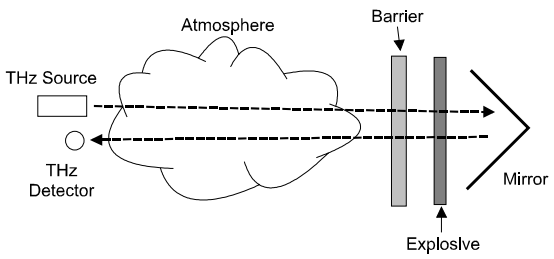

Figure 5. Schematic of THz detection of explosive hidden behind a barrier material using a dual pass transmission geometry.

pulses through 2.4 m of a humid atmosphere, a 1 ps pulse is broadened to a time duration in excess of 30 ps. After 100 m, the pulse duration is well beyond 100 ps [8].

In order to spectroscopically identify an explosive, the THz reflection/transmission of a material must be measured at more than one wavelength. One complication with imaging at different THz frequencies is that the overall spatial resolution of the THz imaging depends on the wavelength of the lowest THz frequency. This is essentially a diffraction effect: the larger THz wavelengths cannot spatially resolve as small an object as the smaller wavelengths. Consequently, when THz images are analysed (using artificial neural networks, for example, section 5) for the spectral presence of an explosive, the edges or boundaries of the explosive are often misidentified.

3.5. Estimation of stand-off range

In determining the effect of target ranges for THz stand-off detection, a detailed analysis of the transmitted THz power, received THz power and noise sources of the detector, background THz radiation and detection method is required. The reader is referred to an extensive discussion of the fundamentals of THz stand-off sensing given by Brown [28]. Brown illustrates the detection limits for several different types of detectors and their application to detection of airborne *Bacillus subtilus* (an anthrax simulant). His calculations show, for example, that a THz differential absorption radar with a Si composite bolometer can detect a 20 m thick anthrax cloud with a particle density of 10^4 cm^{-3} from a distance of 0.5 km. For our purposes, we present a simplified estimate of how the atmospheric, barrier material and sample attenuation determine the effective range of THz detection.

Following [28], the received THz power can be estimated for a transmission geometry as shown in figure 5. A bright THz source illuminates the area under study. The THz radiation is assumed to travel a distance D through the atmosphere. In the transmission geometry, after propagating through the atmosphere, the THz radiation passes through a barrier material (e.g. wood, cardboard and clothing) and through the explosive sample. A mirror redirects the THz radiation back through the explosive, barrier material and atmosphere to the THz receiver. This two-pass geometry is used so that the geometry is comparable to an explosive hidden in a box. In a reflective geometry, the THz radiation would propagate through the barrier material and then reflect from the explosive sample. The reflected light must pass back through the barrier material and atmosphere before being sensed with a THz receiver.

As discussed by Brown [28], the received power in these transmitter–receiver configurations decreases as $\sim 1/D^2$ or slower. This quadradic dependence results from a geometric spreading of the THz beam from the transmitter. Essentially, at suitably long distances the propagating THz waves can be approximated as spherical waves. A factor of $\sim 1/D^4$, which is typically associated with long-range radar applications, is too pessimistic reasonable distances for stand-off THz detection. The extra factor of $\sim 1/D^2$ for radar-type applications results from the assumption of an isotrophic scattering by the target. In essence, the isotropic scattering acts as a point source of radiation.

The power received by the detector in the transmission geometry (figure 5) can be written as

$$P_\mathrm{r} = A_\mathrm{r}\left[\frac{P_0}{\Theta(2D)^2}\right] \mathrm{e}^{-2\alpha_\mathrm{b}L_\mathrm{b}}\, \mathrm{e}^{-2\alpha_\mathrm{a}D}\, \mathrm{e}^{-2\alpha_\mathrm{e}L_\mathrm{e}} \qquad (1)$$

where P_0 is the transmitter power, Θ is the solid angle in which the transmitted power is directed, A_r is the effective area of the receiver, L_b and L_e are the thicknesses of the barrier and explosive layers respectively and α_b, α_a and α_e are the attenuation coefficients of the barrier material, atmosphere and explosive, respectively. The equation accounts for the geometric expansion of the illuminating THz beam (term in brackets), and the attenuation of the barrier, explosive and atmosphere. The factor of 2 in the exponents results from a double pass through the attenuating mediums.

To estimate the effective range of a THz stand-off detector, the received THz power as a function of distance is calculated from equation (1). Rather than specifying a specific detection method/THz detector combination to compute the receiver NEP and bandwidth, we assume that the total receiver noise limit is $P_\mathrm{min} = 3 \times 10^{-11}$ W. (This receiver noise limit is comparable to what is achievable with room temperature photoconductive THz receiver modules [7].) For these calculations, a 0.8 THz frequency within the $\sim$0.8 THz transmission band in the atmosphere is assumed. This transmission band also corresponds to the maximum absorption peak in the RDX THz spectra (40 dB mm^{-1} at 0.8 THz) [14].

The THz source is assumed to emit a power $P_\mathrm{o} = 100$ mW within a constant solid angle of $\Theta = 1.6 \times 10^{-3}$ steradians. This assumed power level represents an advance in the current state-of-the-art compact/portable THz source technology. (A summary of state-of-the-art THz sources can be found in [55].) However, it is anticipated that this milestone may be achievable through recent research and development initiatives [56] in compact/portable THz source development. In terms of the lower power levels that may be achievable with other THz generation techniques, the lower initial power levels shift the received power levels downwards in figures 6–8. For example, a 1 mW backward wave oscillator (BWO) source shifts the calculated received power curves downwards 20 dB. This implies that current lower power sources might be used for shorter stand-off distances, while the detection of explosives at significant stand-off distances would require substantial development in compact/high power THz sources.

The area of illumination in the calculations at a distance of 25 m is assumed to be 1 m^2. This area is chosen to be large enough that in principle this area could be imaged using a THz

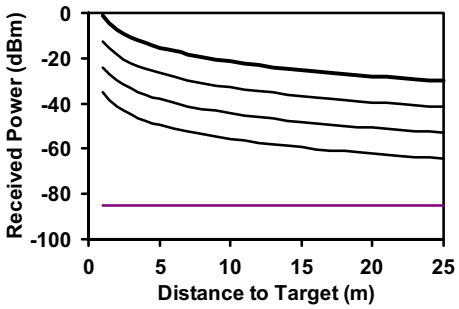

Figure 6. Calculation of detected THz power through a Ski jacket (1.9 dB m^{-1}) of varying thickness 0, 3, 6 and 9 mm (curves top to bottom). Zero thickness corresponds to no jacket. The attenuation coefficients of the barrier materials, atmosphere and air are taken from experimental measurements. The horizontal line corresponds to the estimated P_{min} of the system. The thickness of the explosive is 0.1 mm. Note that the detected power is sufficiently large to detect the thin layer of explosive even at a distance of 25 m.

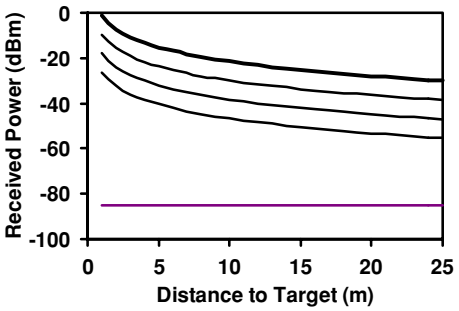

Figure 7. Calculation of detected THz power through a corrugated cardboard (1.4 dB mm^{-1}) of 0, 3, 6 and 9 mm thickness. The attenuation coefficients of the barrier materials, atmosphere and air are taken from experimental measurements. Note that the 0.1 mm thick RDX level is easily detectable up to distances of 25 m even with multiple layers of the barrier material.

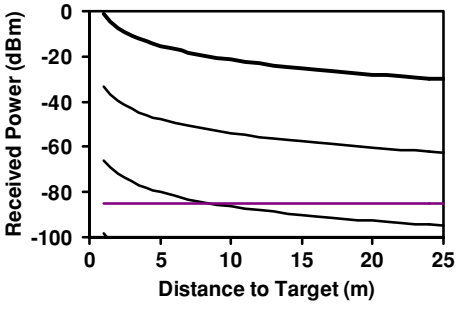

Figure 8. Calculation of detected THz power through a wool sweater (5.4 dB mm^{-1}) of thickness 0, 3, 6 and 9 mm for a transmission geometry. The attenuation coefficients of the barrier materials, atmosphere and air are taken from experimental measurements. Note that since the wool sweater is so much more scattering (high attenuation coefficient) compared to other materials, the effective range is greatly reduced for multiple layers. An explosive hidden behind a 3 mm thick sweater can be detected up to 25 m. A 6 mm sweater restricts the effective range to <8 m.

imaging array. If a point detection system is required, the divergence of the illuminating source could be reduced with a commensurate reduction in the required THz illuminating power. The values for atmospheric attenuation used in this calculation correspond to 50 dB km^{-1} attenuation at 0.8 THz. The attenuation coefficients for the barrier materials are based on experimental data. The detector area is assumed to be 1 cm^2.

Figures 6–8 show the received THz power and P_{min} for a variety of barrier materials for a transmission geometry. Similar curves can be generated for a reflective geometry. The curves indicate the received THz power for various barriers and thicknesses. The horizontal line indicates the assumed P_{min} for the receivers. The location of D for which the received power and NEP curves intersect gives an estimated maximum range of the THz system.

The separation between the curves representing different barrier thicknesses is indicative of the barrier material's attenuation (dB mm^{-1}). Note that as the distance to the target decreases, the power requirements (and detector NEP requirements) are not as stringent as they would be for stand-off detection. From the above data, note that the wool sweater presents a challenge for THz stand-off detection of explosives. This material is not very transparent to THz radiation (attenuation 5.4 dB mm^{-1}) most likely due to scattering of the THz radiation by the wool fibres in the sweater.

4. Interferometric imaging

Interferometric imaging [57–60] has been suggested as a novel imaging modality for stand-off detection of explosives, weapons and other threats. The interferometric THz imaging array design does not require a particular coherent or incoherent source of THz. It is flexible enough to utilize an electronic THz source, a laser-based THz illuminating source or incoherent ambient THz radiation that may be present. The THz imaging array approach should have sufficient spatial resolution to detect centimetre-sized concealed explosives from stand-off distances. A longer-term advantage is that interferometric imaging may produce more information than a single line-of-sight system. With repeated measurements, it should be possible to apply imaging processing/computational techniques to multiple images and THz sources to aid noise and false alarm reduction. In the millimetre wave range, it is anticipated that synthetic aperture techniques could enable imaging systems (1 m aperture) that are light weight and only a few wavelengths in thickness [61].

To perform imaging of THz in real time, the basic technique of radio interferometry [62] is employed for which signals at two or more points in space (the aperture plane) are brought together with the proper delay and correlated both in phase and in quadrature to produce cosine and sine components of the brightness distribution. This technique thus measures both amplitude and phase of the incoming signals. If measured from a sufficient number of points in the aperture plane, the original brightness distribution can be synthesized (imaged) through standard Fourier inversion. The raw images after inversion can be improved through standard image reconstruction techniques (e.g. CLEAN or MEM) to reduce ambiguities (called sidelobes) in the images.

The imaging interferometer consists of an array of individual detectors. As a wavefront of THz radiation encounters the array, each pair of detectors measures one spatial Fourier component of the incoming THz radiation as determined by the separation of the detector pair, otherwise

known as a baseline. Each spatial Fourier component is represented by a point in the Fourier transform plane (called the u–v plane). In order to determine a spatial Fourier component and consequently the direction of the incoming THz wavefront, the delay in arrival time of the wavefront between a pair of antennas must be measured. For a single point source, this measurement will yield an angle at which the object is located from the detector. In order to image the source, additional measurements with baselines at other spacings and orientations must be carried out. Image quality is mainly dependent on detector placements in the imaging array. Since every baseline determines a singe spatial frequency, it is best to have a zero-redundant [61] array.

For a given number of detectors N, there are $N(N-1)/2$ possible pair combinations. An image is generated from the spatial Fourier components of all the different pair combinations. The quality of an image depends on the coverage of the u–v plane, which in turn depends on the arrangement of the detecting elements of the interferometer. The primary concern in designing the configuration of antennas is to obtain uniform and efficient coverage of the u–v plane over a range determined by the required angular resolution. Efficient u–v plane coverage with a small number of detectors may be achieved by rotating the array about a fixed axis. If measurements are made 20 times during the rotation of an N-element array, the equivalent number of baselines will be $20N(N-1)/2$. This can either lead to improved image quality or equivalently to a reduction in the number of required detectors in the array for a given image quality.

With radio wave interferometric imaging of astronomical sources [62], typically it is assumed that the incoming radiation are planar waves. This 'far-field' assumption is used for synthetic imaging and simplifies the imaging reconstruction process. However, most stand-off THz applications do not fall in the 'far-field' limit, and the simplified inverse Fourier transform of the electric field correlation needs to be modified [58].

For interferometric detection, the correlation of the electric fields at the various pairs of detectors is calculated. It can be shown that the mutual coherence function of the electric fields at detector placements $\mathbf{r}_1 = (x_1, y_1)$ and $\mathbf{r}_2 = (x_2, y_2)$ can be written as [58, 62]

$$C_{1,2} = \int_S \frac{\sigma_E(\mathbf{r}')\exp(\mathrm{i}k(r_1 - r_2))}{r_1 r_2}\,\mathrm{d}S', \tag{2}$$

where $\sigma_E(\mathbf{r}')$ is the time-averaged intensity of the surface at $\mathrm{d}S'$, and the integral is over the surface S of the radiating source. Assuming that $|\mathbf{r}' - \mathbf{r}|/Z_0 \ll 1$, $r_1 - r_2$ becomes

$$r_1 - r_2 = \frac{x_1^2 - x_2^2 + y_1^2 - y_2^2}{2Z_0} + \frac{(x_2 - x_1)x' + (y_2 - y_1)y'}{Z_0} \tag{3}$$

where Z_0 is the distance along the z axis between the object and the imaging array, and x', y' and z' locate the spatial coordinates of the object. Using the following definitions, $u = k(x_1 - x_2)/2\pi$, $v = k(y_1 - y_2)/2\pi$, $\xi = x'/Z_0$ and $\eta = y'/Z_0$, the coherence function of equation (2) can be cast into the form [62]

$$C_{1,2}(u, v) = \exp(\mathrm{i}\delta)\int_{-\infty}^{\infty}\int_{-\infty}^{\infty}\sigma_E(\xi, \eta) \times \exp(-\mathrm{i}2\pi(u\xi + v\eta))\,\mathrm{d}\xi\,\mathrm{d}\eta \tag{4}$$

Table 2. Estimated phase error δ from imaging a 2.5 cm object at various distances using 1 THz radiation. The baseline b is an estimate of the physical size of the imaging array. Note that for distances of 5–10 m, the size of the imaging array is 6–12 cm suggesting that a hand-held unit might be achievable.

Z_0 (m)	5	10	50	100	500	1000
b (m)	0.06	0.12	0.6	1.2	6	12
δ	2.4	4.8	24	48	240	480

where the denominator of equation (4) has been approximated as $1/r_1 r_2 \approx 1/Z_0^2$. If an object is in the far-field ($\delta \ll 1$), the phase shift $\delta = k\left(x_1^2 - x_2^2 + y_1^2 - y_2^2\right)/2Z_0$ can be neglected and equation (4) will relate the coherence function in the antenna plane to the brightness distribution of the source(s). By a Fourier transform, the brightness distribution (image) can be reconstructed by measuring the coherence function for a given arrangement of detectors in the sensor array. Imaging with a significant phase shift results in poor image quality (extremely blurred).

The condition for negligible phase shift δ can be approximately expressed as $Z_0 \gg b^2/\lambda$, where b is the largest baseline length of the imaging array and λ is the THz wavelength. As an example, assume that a 2.5 cm object needs to be imaged at various distances. The angular resolution of a planar array can be approximated as $\theta_{\min} = \lambda/b$. At a distance Z_0 away, the lateral spatial resolution is $\Delta L_{\mathrm{lat}} \approx \theta_{\min} Z_0 \approx \lambda Z_0/b$. Using $\delta \approx b^2/Z_0\lambda$ as an estimate for the far-field limit of a planar array, the limit can now be estimated as $\delta \approx Z_0\lambda/\Delta L_{\mathrm{lat}}^2$. In order to maintain a 2.5 cm lateral resolution, table 2 shows the corresponding maximum baseline required and phase error. Note that for this application, the far-field criteria of $\delta \ll 1$ are never satisfied; THz interferometric imaging for stand-off applications *must* include contributions from the near-field.

The 'blurring' of the THz image for stand-off applications can be greatly reduced by changing the arrangement of the detectors in the imaging array. In essence, the arrangement of the detectors in the array must be modified to 'focus' the imaging array at stand-off distances. In particular, it can be shown [58] that in spherical coordinates, the coherence function can be cast into the form of equation (4) where the phase shift is now $\bar{\delta} = kz'(\cos\theta_2 - \cos\theta_1)$. If the near-field phase error $\bar{\delta}$ can be neglected, equation (4) would then relate the coherence function to the brightness distribution of the source. One configuration that eliminates the phase error is to arrange the detectors in a circle. In this configuration, all detectors have the same azimuth angle thereby enforcing $\bar{\delta} = kz'(\cos\theta_2 - \cos\theta_1) = 0$. For this circular arrangement, the first-order phase error vanishes implying clear images with a large depth of focus.

Figure 9 illustrates a simulated 35° field-of-view image of the NJIT logo from a distance of 25 m. The number of detectors in the circular array varies from 49, 100 to 200. Note that as the number of detectors in the array is increased, the image becomes clearer. This is expected since increasing the number of detectors increases the number of Fourier components that can be measured and increases the resolution and reduces the distortion in a reconstructed image. Standard image processing techniques can be used to 'clean' the reconstructed images to reduce the distortion in the

Figure 9. A THz emitting object in the shape of the NJIT logo. The number of detectors in the circular imaging array is $N = 49$, $N = 100$ and $N = 200$ from left to right. The distance to the object is 25 m with a $\sim 35^{\circ}$ field of view. The images are unprocessed (uncleaned). After processing to remove imaging artefacts, the image quality can be dramatically improved.

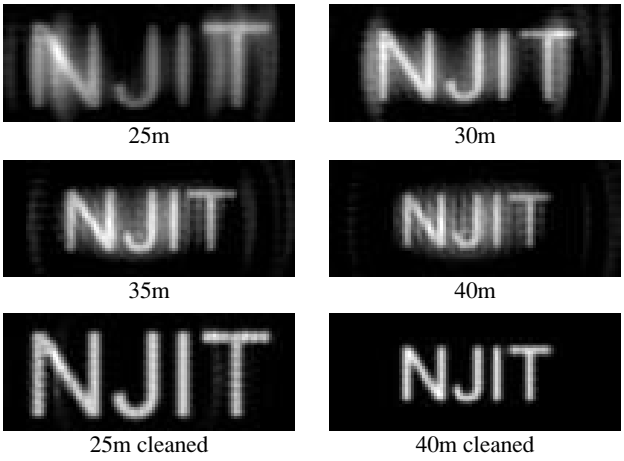

Figure 10. Theoretical calculation of a THz image generated by an interferometric imaging array. The NJIT logo, 0.8 m × 0.3 m^2, is imaged using a circular array of 100 equally spaced detectors with a radius of 0.1 m. The imaging array is optimized for a 25 m distance. Note that the image decreases in size as the target recedes from the imaging array. The bottom two images have been cleaned using the point spread function of the imaging array.

reconstructed images. Note that the 200-element image shows minimal lateral distortions.

The circular array architecture is capable of a large depth of focus larger than ±10% of the distance to the target and a large field of view (35°). Figure 10 illustrates the image of an object as it moves through the optimal focal distance. It should be emphasized that the lateral distortions are not severe nor are they a limiting factor in the THz imaging array performance.

When is it preferable to use an interferometric imaging approach rather than a focal plane approach? What are the trade-offs? To answer this question, we compare the performance of the two types of imaging arrays for imaging a 1 m^2 area with 2.5 cm resolution at a distance of 25 m using the same number of detectors. The number of detectors is chosen to be $N = 57$ so that the number of pixels in the THz image is the same for both imaging methods. In these calculations, it is assumed that the time to digitize or acquire the data from each detector is the same for both the interferometric and focal plane array approach. This is a reasonable assumption, for example, if the same or comparable detectors are used for both approaches. The major differences in the two approaches are that the interferometric imaging array can record the entire THz image at once, while the focal plane array requires the array to scan the object. For this example, the focal plane array would take 30 times longer than the interferometric approach to acquire an image. However, there is a trade-off—roughly 1600 correlations are needed for the interferometric imaging array. This interferometric imaging hardware requirement is not necessary with a focal plane array. In essence, one is trading imaging speed for backend image processing (the correlation).

If there is not a restriction on the time to generate an image (i.e. real-time imaging is not required), one can reduce the required number of detectors for interferometric imaging accordingly. For example, if the interferometric array is scanned (by rotating the array), the equivalent number of pixels in the reconstructed image is $MN(N-1)/2$, where N is the number of detectors in the array and M is the number of unique rotational positions of the array. Assuming 28 different rotation positions for the interferometric array, the corresponding time to acquire an image would be the same for both techniques. However, in order to maintain the number of pixels at ∼1600, only 11 detectors are required in the interferometric approach compared to 57 for the focal plane array approach. This reduction in the number of detectors reduces the required number of correlations from 1600 to 55.

5. THz spectral and image analysis

Terahertz images themselves are generally not sufficient to identify hidden explosives or illegal drugs due to the complicating effects of barrier materials, noise, similarity in THz spectra, etc. Therefore, spectral and image analyses are required to reduce false alarm rates. Two approaches to THz image analysis are discussed here.

5.1. Component pattern analysis

The first method, employed recently by Kawase *et al* [23, 53], uses a matrix form of the Beer–Lambert absorption law in a transmission mode. A two-dimensional sample is raster-scanned by a pulsed, tunable THz source to generate an N rows × L columns image matrix $[I]$, where N is the number of THz frequencies used and L is the number of pixels. The values of $[I]$ are the measured total absorbance at each pixel. Separate absorption experiments with known materials of interest establish the THz spectra both graphically and through the $N \times M$ spectra matrix $[S]$, where M is the number of components. The collection of species can include non-agent materials that can affect the absorptions, e.g., barrier materials with spectra that are typically weakly frequency dependent. The spatial patterns of the agents are contained in the $M \times L$ matrix $[P]$. The values of $[P]$ effectively contain agent concentration information.

Based on the Beer–Lambert law, the matrices are related by

$$[I] = [S][P]. \tag{5}$$

The total absorbance entries of $[I]$ are, in effect, weighted sums of the absorbance of each material at a specific location. For example, if two different agents are present at one location behind a barrier material, assuming spectra for all components exist in $[S]$, then matrix $[P]$ will reveal how much of each

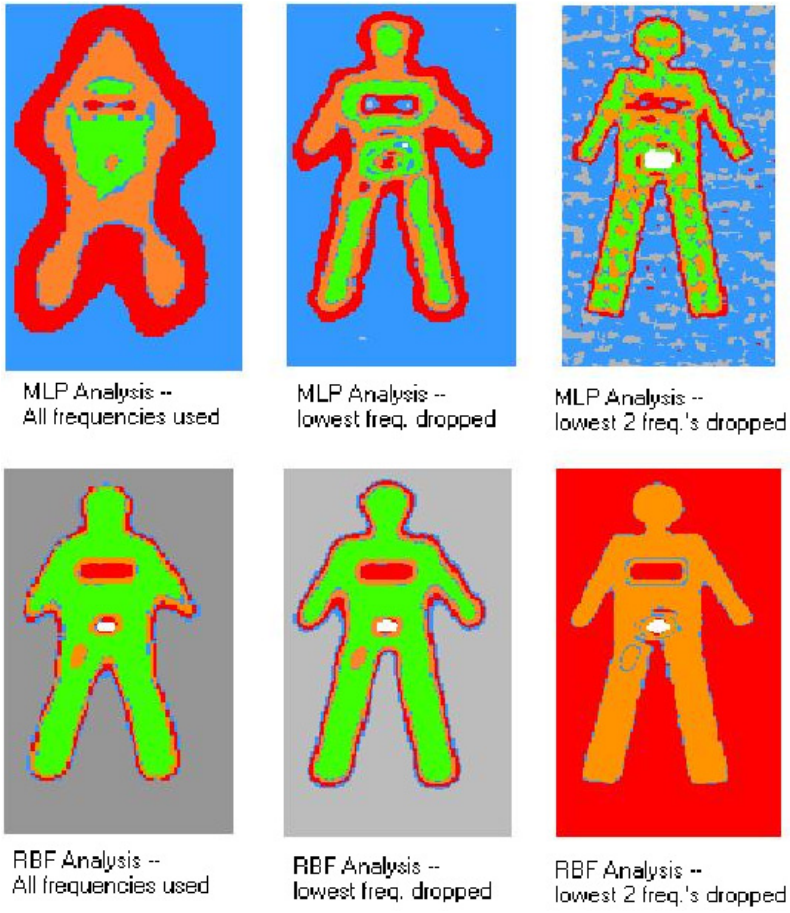

Figure 11. Bitmap of MLP and RBF analyses of bomber problem (print version: white = metal, black = RDX, light grey = background/unknown, medium grey = skin/candy) (online version: white = metal, red = RDX, orange = candy, green = skin, grey = background and blue = unknown).

component is present and in what spatial pattern. The matrix $[P]$ is determined, for cases where $N > M$, from

$$[P] = ([S]^{t}[S])^{-1}[S]^{t}[I] \tag{6}$$

where t indicates matrix transpose, and -1 indicates matrix inverse. Kawase *et al* have successfully used this technique to identify pellets of aspirin and palatinose (a food sweetener), and the illegal drugs, methamphetamine and MDMA, hidden in small plastic bags.

5.2. Artificial neural networks

The second method discussed here uses artificial neural networks (NNs) to analyse the THz images [63], obtained in either reflection or transmission mode, and classify the pixels of the image as to their component material (e.g. explosive, barrier material, metal, skin, etc). An artificial NN is a computational mapping which can be optimized, or 'trained', to detect certain patterns. The algorithm inputs are the reflected/transmitted THz power for a finite number of THz fingerprint frequencies. The NN is trained to recognize the intensity pattern of THz frequencies corresponding to explosives, paper, metal, skin, barrier materials, etc. When an unknown intensity pattern is presented as input, the NN attempts to classify the pattern as one of its known materials based on a library of THz spectra. At present, the NN analyses the image on a pixel-by-pixel basis.

During the training of a NN with a given set of input/output data, a set of internal parameters (weights) is optimized so that the outputs predicted by the NN match the desired outputs to within an acceptable tolerance. Network architectures typically contain a layer of input nodes accepting the input values, one or more hidden layers of nodes and an output layer of nodes. The multilayer perceptron (MLP) and radial basis function (RBF) are two NN architectures that have proved especially useful for THz image analysis. The input values for NN training correspond to spectral intensities at each frequency. The single output for each material of interest is an arbitrarily chosen integer value within a user-defined tolerance. A corresponding colour is also assigned.

As an example of NN analysis, consider a person with RDX explosive attached to their chest under a shirt (assumed transparent to THz). Both MLP and RBF architectures were tested, with colour bitmap results in figure 11. The MLP results are very poor, with little spatial resolution and little correctly identified. The RBF results show a much-improved spatial resolution. As with the MLP, each object is correctly identified as evident by the central major-sized colour. The degree of inaccuracies, as evidenced by minor-sized colours, is much reduced. The evidence of 'unknown' results is effectively

gone. The improved performance of the RBF is consistent with its preferred capability with 'classification' problems, especially with limited data. Objects are correctly identified, with slight colour inaccuracies in border transition zones (i.e. edges). Each object—correctly identified in each case—is visible as a central major-sized colour generally surrounded by other colour(s)—an artefact corresponding to transition zones between the object and the background. Edge effect artefacts were also observed by Kawase *et al* [23, 53].

For sensitivity testing, the bomber problem was redone with the NNs trained with only the four highest spectral frequencies. Figure 11 shows that the spatial resolution is improved, with some of the skin and RDX now visible for the MLP case. This improvement in spatial resolution is due to the removal of the lowest THz frequency that corresponds to the poorest spatial resolution. However, the colours are still widely wrong. However, with an improved spatial resolution, the RBF again accurately identified the components of the bomber. Dropping the two lowest frequencies (0.03 and 0.08 THz) degrades the performances of both architectures. The MLP does not correctly identify the candy, and poorly shows the RDX, though the metal buckle is now visible. The RBF incorrectly identifies the person as being covered in or made of candy, though the RDX is correctly revealed.

5.3. Artefacts

Artefacts challenge the ability of THz image analysis methods. For example, rings appear on the edges of THz images of various pellets analysed by component pattern analysis [23, 53]. These rings were attributed to differences in THz wave spot size at each frequency. Similarly, edge effects were observed in the analysis of simulated interferometric THz images (see figure 11) due to the differing spatial resolution associated with each THz wavelength. These edge effects appear where there is a transition from one material to another within the images.

6. Future challenges and outlook

THz detection and imaging has shown great promise for security applications since many non-metallic, non-polar materials are transparent to THz radiation, target compounds have characteristic THz spectra that can be used to identify these compounds and THz radiation poses no health risk for scanning of people. Several system architectures for proximity detection are well-advanced. For proximity scanning, many modalities (e.g. CW or pulsed) should be competitive. The key issue remaining for proximity detection is to increase the frame rate for real-time imaging. Other issues that need to be addressed as THz technology moves out of the research laboratory and into the field include issues of portablity, hand-held size, cost and power requirements.

While crystalline, high energy explosives have characteristic THz fingerprint spectra that can be used to identify these threats, home-made ammonium nitrate bombs and other improvised explosive devices could pose a challenge to THz security applications since these materials can have featureless THz spectra below 3 THz.

The biggest challenge to THz security applications is stand-off detection. As the stand-off distance increases, one must consider the effect of the humid atmosphere, dust, smoke, etc as well as possible barrier materials. At stand-off distances, picosecond pulsed measurements become problematic. In order to overcome the attenuation losses of barrier materials and the atmosphere, higher power sources need to be developed. In conjunction, compatible low-noise THz receivers need further development.

To date, most work on THz stand-off detection assumes that the THz power reflected from barrier materials (i.e. backscatter) can be ignored. This is certainly a valid assumption in the transmission mode or using a close proximity time-domain technique for which the reflections do not appear in the detected time window. In the reflection mode, one must detect the reflected power from the threat material and differentiate that contribution from the reflected light from barrier materials. For a fairly transparent material (e.g. corrugated paper figure 6 or ski jacket figure 7), the amount of diffusively reflected radiation from the barrier material should be fairly small and easily distinguished from the reflection from the explosive. For highly scattering material, such as the wool sweater, the diffuse reflection from the front surface of the sweater is much more problematic since the 'real' reflection from the explosive is highly attenuated—since it passes through the attenuating sweater—as compared to the reflection from the sweater. This problem may possibly be circumvented by using a differential reflection technique. This is accomplished by measuring the difference in reflection of two THz frequencies. This differential technique effectively removes the contribution of the reflections from the barrier materials and amplifies the THz spectral presence of the threat material. A similar technique has been proposed by Woolard *et al* for the remote THz detection of bioagent clouds [10, 15, 28].

Acknowledgments

The authors thank the Technical Service Working Group (TSWG) Explosives Directorate (Contract N41756-04-C-4163), the US Army (Contract DAAD19-03-C-0137) and the Foundation at NJIT for supporting their work in THz imaging. Discussions with Professor J M Joseph are gratefully acknowledged.

References

[1] Loffler T, Siebert K, Czasch S, Bauer T and Roskos H 2002 Visualization and classification in biomedical terahertz pulsed imaging *Phys. Med. Biol.* **47** 3847–52

[2] Walker G C, Berry E, Zinov'ev N N, Fitzgerald A J, Miles R E, Martyn C and Smith M A 2003 *Terahertz Imaging and International Safety Guideline* www.comp.leeds.ac.uk/comir and GR/N39678: *Medical Terahertz Pulsed Imaging: The Interaction of Terahertz Radiation with Biological Tissue* www.comp.leeds.ac.uk/comir/research/terahertz/GRN39678.html

[3] Berry E 2003 Risk perception and safety issues *J. Biol. Phys.* **29** 263–7

[4] Clothier R H and Bourne N 2003 Effects of THz exposure on human primary keratinocyte differentiation and viability *J. Biol. Phys.* **29** 179–85

[5] Scarfi M R *et al* 2003 THz exposure of whole blood for the study of biological effects on human lymphocytes *J. Biol. Phys.* **29** 171–7

[6] For example, see Appleby R, Wikner D A, Trebits R and Kurtz J L (ed) 2003 Passive millimeter-wave imaging technology VI and radar sensor technology VII *Proc. SPIE* **5077**

[7] Zimdars D A and White J S 2004 Terahertz reflection imaging for package and personnel inspection *Proc. SPIE* **5411** 78
Zimdars D A 2003 Fiber-pigtailed terahertz time-domian spectroscopy instrumentation for package inspection and security imaging *Proc. SPIE* **5070** 108

[8] Yuan T, Liu H, Xu J, Al-Douseri F, Hu Y and Zhang X 2003 *Proc. SPIE* **5070** 28

[9] Heimer T A and Heilweil E J 2002 *Bull. Chem. Soc. Japan* **75** 899–908

[10] Woolard D L *et al* 1997 *J. Appl. Toxicol.* **17** 243

[11] De Lucia F C 2003 Spectroscopy in the terahertz spectral region *Sensing with Terahertz Radiation* ed D Mittleman (Berlin: Springer)

[12] Tribe W R, Newnham D A, Taday P F and Kemp M C 2004 Hidden object detection: security applications of terahertz technology *Proc. SPIE* **5354** 168

[13] Kemp M C, Taday P F, Cole B E, Cluff J A, Fitzgerald A J and Tribe W R 2003 *Proc. SPIE* **5070** 44

[14] Huang F, Schulkin B, Altan H, Federici J, Gary D, Barat R, Zimdars D, Chen M and Tanner D B 2003 Terahertz study of 1,3,5-trinitro-s-triazine (RDX) by time domain spectroscopy and FTIR *Appl. Phys. Lett.* **83** 2477

[15] Woolard D, Globus T, Brown E, Werbos L, Gelmont B and Samuels A 2001 *Proc. 5th Joint Conf. Standoff Detection for Chemical and Biological Defense (Williamsburg, VA)*

[16] Cook D J, Decker B K, Maislin G and Allen M G 2004 Through container THz sensing: applications for explosive screening *Proc. SPIE* **5354** 55

[17] Cohen R W, Cody G D, Coutts M D and Abeles B 1973 *Phys. Rev.* B **8** 3689

[18] Federici J F and Grebel H 2003 Characteristics of nano-scale composites at THz and IR spectral regions *Sensing Science and Technology at THz Frequencies, Volume II. Emerging Scientific Applications & Novel Device Concepts* ed D Woodard, M Shur and W Loerop (Hackensack, NJ: World Scientific)
Altan H, Huang F, Federici J F, Lan A and Grebel H 2004 Optical and electronic characteristics of single walled carbon nanotubes and silicon nanoclusters by THz spectroscopy *J. Appl. Phys.* **96** 6685

[19] Campbell M B and Heilweil E J 2003 Noninvasive detection of weapons of mass destruction using THz radiation *Proc. SPIE* **5070** 38

[20] Fitch M J, Schauki D, Kelly C A and Osiander R 2004 Terahertz imaging and spectroscopy for landmine detection *Proc. SPIE* **5354** 45

[21] Rice B M and Chabalowski G F 1997 *J. Phys. Chem.* A **101** 8720–6

[22] Bandyopadhyay A, Sengupta A, Huang F, Federici J F, Barat R B, Gary D E, Chen M and Tanner D B 2005 Impact of grain size dependent scattering on terahertz absorption spectra *Appl. Opt.* submitted

[23] Kawase K, Ogawa Y and Watanabe Y 2003 Non-destructive terahertz imaging of illicit drugs using spectral fingerprints *Opt. Express* **11** 2549

[24] Taday P F, Bradley I V, Arnone D D and Pepper M 2003 *J. Pharm. Sci.* **92** 831–8

[25] Watanabe Y, Kawase K and Ikari T 2003 Component spatial pattern analysis of chemicals using terahertz spectral imaging *Appl. Phys. Lett.* **83** 800

[26] Bjarnason J E, Chan T L J, Lee A W M, Celis M A and Brown E R 2004 Millimeter-wave, terahertz, and mid-infrared transmission through common clothing *Appl. Phys. Lett.* **85** 519

[27] Osiander R, Miragliotta J A, Jiang Z, Xu J and Zhang X C 2003 Mine field detection and identification using THz spectroscopic imaging *Proc. SPIE* **5070** 1
Spicer J B, Dagdigian P, Osiander R, Miragliotta J A, Zhang X C, Kersting R, Crosley D R, Hanson R K and Jeffries J 2003 *Proc. SPIE* **5089** 1088
Chen Y, Liu H, Deng Y, Veksler D, Shur M, Zhang X-C, Schauki D, Fitch M J and Osiander R 2004 Spectroscopic characterization of explosives in the far infrared region *Proc. SPIE* **5411** 1

[28] Brown E R 2003 Fundamentals of terrestrial millimeter-wave and THz remote Sensing *Terahertz Sensing Technology, vol 2: Emerging Scientific Applications & Novel Device Concepts* ed D L Woolard, W R Loerop and M S Shur (Singapore: World Scientific)

[29] van der Weide D W 2003 Electronic sources and detectors for wideband sensing in the terahertz regime *Sensing with Terahertz Radiation* ed D Mittleman (Berlin: Springer)

[30] Chen Y, Liu H, Deng Y, Schauki D, Fitch M J, Osiander R, Dodson C, Spicer J B, Shur M and Zhang X-C 2004 THz spectroscopic investigation of 2,4-dinitrotoluene *Chem. Phys. Lett.* submitted

[31] Shen Y, Taday P F and Kemp M C 2004 Terahertz spectroscopy of explosive materials *Proc. SPIE* **5619** 82

[32] For example, see Hu B B and Nuss M C 1995 *Opt. Lett.* **20** 1716–8

[33] Mittleman D M, Hunsche S, Boivin L and Nuss M C 1997 *Opt. Lett* **22** 904

[34] O'Hara J and Grischkowsky D 2002 Synthetic phased-array terahertz imaging *Opt. Lett.* **27** 1070

[35] O'Hara J and Grischkowsky D 2004 Quasi-optic synthetic phased-array terahertz imaging *J. Opt. Soc. Am.* B **21** 1178–91

[36] Hu B B and Nuss M C 1995 Imaging with terahertz waves *Opt. Lett.* **20** 1716–8

[37] McKlatchy K, Reiten M T and Cheville R A 2001 Time resolved synthetic aperture terahertz impulse imaging *Appl. Phys. Lett.* **79** 4485–7

[38] Wu Q, Hewitt T D and Zhang X C 1996 Two-dimensional electro-optic imaging of THz beams *Appl. Phys. Lett.* **69** 1026–8

[39] Jiang Z and Zhang X C 1998 Single-shot spatiotemporal terahertz field imaging *Opt. Lett.* **23** 1114–6

[40] McIntosh K A, Brown E R, Nichols K B, McMahon O B, DiNatale W F and Lyszczarz T M 1995 Terahertz photomixing with diode lasers in low-temperature-grown GaAs *Appl. Phys. Lett* **67** 3844

[41] Duffy S M, Verghese S and McIntosh K A 2002 Photomixers for continuous-wave terahertz radiation *Sensing with Terahertz Radiation* ed D Mittleman (Berlin: Springer)

[42] Chan T L J, Bjarnason J E, Lee A W M, Celis M A and Brown E R 2004 Attenuation contract between biomolecular and inorganic materials at terahertz frequencies *Appl. Phys. Lett.* **85** 2523

[43] Loffler T, Siebert K J, Quast H, Hasegawa N, Lota G, Wipe R, Hahn T, Thomson M, Leonhardt R and Roskos H G 2004 All-optoelectronic continuous-wave terahertz systems *Phil. Trans. R. Soc.* A **362** 263

[44] Siebert K J, Loffler T, Quast H, Thomason M, Bauer T, Leonhardt R, Czasch S and Roskos H G 2002 All optoelectronic continuous wave THz imaging for biomedical applications *Phys. Med. Biol.* **47** 2743

[45] Siebert K J, Quast H, Leonhardt R, Loffler T, Thomson M, Bauer T, Roskos H G and Czasch S 2002 Continuous-wave all-optoelectronic terahertz imaging *Appl. Phys. Lett.* **80** 3003

[46] Kleine-Ostmann T, Knobloch P, Koch M, Hoffman S, Breede M, Hofmann M, Hain G, Pierz K, Sperling M and Donhuijsen K 2001 Continuous-wave THz imaging *Electron. Lett.* **37** 1461

[47] Gregory I S, Tribe W R, Cole B E, Baker C, Evans M J, Bradley I V, Linfiled E H, Davies A G and Missous M 2004 Phase sensitive continuous-wave THz imaging using diode lasers *Electron. Lett.* **40** 143

[48] Bjarnason J E, Chan T L J, Lee A W M, Brown E R, Driscoll D C, Hanson M, Gassard A C and Muller R E 2004 ErAs:GaAs photomixer with two-decade tunability and 12 μW peak output power *Appl. Phys. Lett.* **85** 3983

[49] Verghese S, McIntosh K A and Brown E R 1997 *Appl. Phys. Lett.* **71** 2743

[50] Ryzhii V, Khmyrova I and Shur M 2002 Terahertz photomixing in quantum well structures using resonant excitation of plasma oscillations *J. Appl. Phys.* **91** 1875
Ryzhii V, Khmyrova I, Satou A, Vaccaro P O, Aida T and Shur M 2002 Plasma mechanism of terahertz photomixing in high-electron mobility transistor under interband photoexcitation *J. Appl. Phys.* **92** 5756

[51] Malcoci A, Stohr A, Sauerwald A, Schulz S and Jager D 2004 Waveguid and antenna coupled traveling-wave 1.55 μm photodetectors for optical (sub)millimeter-wave generation *Proc. SPIE* **5466** 202

[52] Nahata A, Yardley J T and Heinz T F 2002 *Appl. Phys. Lett.* **81** 963

[53] Kawase K, Ogawa Y and Watanabe Y 2004 Component pattern analysis of chemicals using multispectral THz-imaging system *Proc. SPIE* **5354** 63

[54] Zimdars D and White J S 2004 Terahertz reflection imaging for package and personnel inspection *Proc. SPIE—Int. Soc. Opt. Eng.* **5411** 78

[55] Krozer V *et al* 2004 Optical far-IR wave generation—state-of-the-art and advanced device structures *Proc. SPIE* **5466** 178

[56] Rosker M and Palmer D 2004 Perspective on DARPA needs and initiatives in terahertz systems and technologies Presented at the *Terahertz Systems Conference (Washington, DC, 6–7 Dec.)*

[57] Schulkin B, Huang F, Gary D, Barat R and Federici J 2005 *J. Appl. Phys.* submitted

[58] Walsh K P, Schulkin B, Gary D, Federici J F, Barat R and Zimdars D 2004 Terahertz near-field interferometric and synthetic aperture imaging *Proc. SPIE* **5411** 9

[59] Federici J F, Gary D, Schulkin B, Huang F, Altan H, Barat R and Zimdars D 2003 Terahertz imaging using an interferometric array *Appl. Phys. Lett.* **83** 2477

[60] Federici J F, Gary D, Schulkin B, Huang F, Altan H, Barat R and Zimdars D 2003 *Proc. Int. Symp. Spectral Sensing Research (Santa Barbara, CA)*

[61] Salmon N A, Hayward S, Walke R L and Appleby R 2003 Electronic scanning for passive millimeter wave imaging *Proc. SPIE* **5077** 71

[62] Thompson A R, Moran J M and Swenson G W 2001 *Interferomtetry and Synthesis in Radio Astronomy* 2nd edn (New York: Wiley Interscience)

[63] Oliveira F, Barat R, Schulkin B, Huang F, Federici J, Gary D and Zimdars D 2004 Analysis of THz spectral images of explosives and bio-agents using trained neural networks *Proc. SPIE* **5411** 45
Oliveira F, Barat R, Schulkin B, Federici J F, Gary D and Zimdars D A 2003 Neural network analysis of terahertz spectra of explosives and bio-agents *Proc. SPIE* **5070** 60